

Observation of the Dalitz Decay $D_s^{*+} \rightarrow D_s^+ e^+ e^-$

Souvik Das¹

(CLEO Collaboration)

¹*Cornell University*

(Dated: March 4, 2011)

Using 586 pb⁻¹ of e^+e^- collision data acquired at $\sqrt{s} = 4.170$ GeV with the CLEO-c detector at the Cornell Electron Storage Ring, we report the first observation of $D_s^{*+} \rightarrow D_s^+ e^+ e^-$ with a significance of 5.3σ . The ratio of branching fractions $\mathcal{B}(D_s^{*+} \rightarrow D_s^+ e^+ e^-)/\mathcal{B}(D_s^{*+} \rightarrow D_s^+ \gamma)$ is measured to be $[0.72_{-0.13}^{+0.15}(\text{stat}) \pm 0.10(\text{syst})]\%$, which is consistent with theoretical expectations.

PACS numbers: 13.20.Fc, 13.40.Hq

Dalitz decays [1], in which a virtual photon is internally converted to an e^+e^- pair, have been observed in several vector-to-pseudoscalar decays of light mesons (e.g., $\omega \rightarrow \pi^0 e^+ e^-$, $\phi \rightarrow \pi^0 e^+ e^-$, and $\phi \rightarrow \eta e^+ e^-$) [2]. However, such decays have not been observed in electromagnetic decays of mesons containing charm or bottom quarks. In this Letter we report the first observation of such a decay, $D_s^{*+} \rightarrow D_s^+ e^+ e^-$, and a measurement of its branching fraction. Details of this analysis can be found in Ref. [3]. Only two decay modes of the D_s^{*+} have been previously observed, the dominant $D_s^{*+} \rightarrow D_s^+ \gamma$ mode and the isospin-violating $D_s^{*+} \rightarrow D_s^+ \pi^0$ [4] decay. Their branching fractions have been determined by the PDG [2] from measurements of the ratio $\mathcal{B}(D_s^{*+} \rightarrow D_s^+ \pi^0)/\mathcal{B}(D_s^{*+} \rightarrow D_s^+ \gamma)$ and the assumption that they are the only D_s^{*+} decay modes.

The expected D_s^{*+} Dalitz decay rate may be calculated by treating the photon from $D_s^{*+} \rightarrow D_s^+ \gamma$ as virtual and coupling it to an e^+e^- pair. The ratio

$$R_{ee} \equiv \mathcal{B}(D_s^{*+} \rightarrow D_s^+ e^+ e^-)/\mathcal{B}(D_s^{*+} \rightarrow D_s^+ \gamma) \quad (1)$$

may then be written in differential form as [5]

$$\begin{aligned} \frac{dR_{ee}}{dq^2} &= \frac{\alpha}{3\pi q^2} \left| \frac{f(q^2)}{f(0)} \right|^2 \left[1 - \frac{4m_e^2}{q^2} \right]^{\frac{1}{2}} \left[1 + 2 \frac{m_e^2}{q^2} \right] \\ &\times \left[\left(1 + \frac{q^2}{A} \right) - \frac{4m_{D_s^*}^2 q^2}{A^2} \right]^{\frac{3}{2}}, \end{aligned} \quad (2)$$

where q is the four-momentum of the virtual photon, m_x represents the mass of particle x , $A \equiv m_{D_s^*}^2 - m_{D_s}^2$, and $f(q^2)$ is the transition form factor for D_s^{*+} to D_s^+ . Motivated by vector-meson dominance, we use $f(q^2)/f(0) = (1 - q^2/m_\phi^2)^{-1}$. Integrating Eq. (2), we obtain a prediction of $R_{ee} = 0.65\%$.

We use 586 pb⁻¹ of e^+e^- collision data with \sqrt{s} near 4.170 GeV acquired by the CLEO-c detector at the Cornell Electron Storage Ring which produced $\approx 5.6 \times 10^5$ $e^+e^- \rightarrow D_s^\pm D_s^{*\mp}$ events. The CLEO-c detector is equipped with a CsI(Tl) calorimeter [6] to detect photons and determine their directions and energies, and two concentric cylindrical wire drift chambers [7] to track the

trajectory of charged particles. The tracking chambers operate in an axial 1 T magnetic field to provide momentum measurements. The beam pipe and the drift chambers present under 2% of a radiation length of material, minimizing multiple scattering of charged particles and photon conversions. Charged hadron identification is achieved using energy loss (dE/dx) in the drift chambers and Cherenkov radiation in the RICH detector [8, 9].

The default Kalman filter track reconstruction used to process CLEO data include corrections for dE/dx and multiple scattering in the beam pipe and detector material, assuming each track has the mass of a pion, kaon, and proton. The e^\pm tracks in this analysis are rather soft, with energies below 150 MeV, where dE/dx is very different from that of any of those three mass hypotheses. Therefore, to improve sensitivity, we reprocess events containing at least one exclusively reconstructed D_s^+ candidate, adding an e^\pm mass hypothesis for each charged particle.

We fully reconstruct $D_s^{*+} \rightarrow D_s^+ e^+ e^-$ candidates with D_s^+ candidates reconstructed through the nine distinct modes listed in Table I. Charge conjugate modes are also included. Candidates for K_S^0 and η are reconstructed through their decays to $\pi^+\pi^-$ and $\gamma\gamma$, respectively. Measurement of R_{ee} instead of the absolute branching fraction $\mathcal{B}(D_s^{*+} \rightarrow D_s^+ e^+ e^-)$ bypasses any need for estimating the total number of D_s^{*+} produced and minimizes systematic uncertainties stemming from reconstruction of the D_s^+ .

To avoid biases, the analysis is performed blind by establishing selection criteria optimized individually in each of the D_s^+ decay modes for maximum signal significance using Monte Carlo simulated samples of signal and background processes. The decay chain of signal events $e^+e^- \rightarrow D_s^{*+} D_s^-; D_s^{*+} \rightarrow D_s^+ e^+ e^-$ are simulated with full angular correlations. Simulated samples of all $e^+e^- \rightarrow q\bar{q}$ processes at 4.170 GeV where $q = u, d, s$, or c are used for background. The reconstructed e^+e^- tracks are required to pass within 5 cm of the interaction point in the direction parallel to the beam-axis and within 5 mm of the beam-axis in the transverse directions. The dE/dx of each e^\pm candidate is required to

be within 3σ of that expected for electrons. All charged pions and kaons in the D_s^+ decay chain are identified as such using a combination of dE/dx and RICH information as in Ref. [10]. We require the reconstructed D_s^+ mass M_{D_s} to be within a mode-dependent region around the known D_s^+ mass [2] consistent with the resolution of the detector. We define the beam-constrained mass of the D_s^{*+} by $M_{BC} \equiv \sqrt{E_{D_s^*}^2 - \mathbf{p}_{D_s^*}^2}$, where $E_{D_s^*}$ is the energy of the D_s^{*+} calculated from the beam energy and $\mathbf{p}_{D_s^*}$ is the three-momentum of the D_s^{*+} measured from its decay daughters. We select events with M_{BC} and $\delta M \equiv M_{D_s^*} - M_{D_s}$ consistent with the known D_s^{*+} and D_s^+ masses [2].

A significant background to the observation of $D_s^{*+} \rightarrow D_s^+ e^+ e^-$ arises from $D_s^{*+} \rightarrow D_s^+ \gamma$ events where the γ converts into an $e^+ e^-$ pair in the material of the beampipe or drift chambers. We reject much of this background using the following criteria for the e^\pm tracks. We define the d_0 of a track as the distance of closest approach of the track to the beam axis. Its sign depends on the charge of the track and whether the origin of the $x-y$ plane falls within the circle of the track in that plane. We require the difference between the d_0 of the e^+ and e^- tracks, $\Delta d_0 = d_0^{e^-} - d_0^{e^+}$, to exceed -5 mm. Denoting the azimuthal angle measured at the point of closest approach of a track to the beam axis by ϕ_0 , we also require $\Delta\phi_0 = \phi_0^{e^-} - \phi_0^{e^+} < 0.12$.

These selection criteria are applied on simulated samples of our signal to obtain the selection efficiencies for signal events ϵ_{ee}^i , where i stands for one of the nine decay modes of the D_s^+ used in this analysis. They are applied to data in order to obtain the yields of events y_{ee}^i . These numbers are presented in Table I for each decay mode of the D_s^+ .

Having established selection criteria using simulated samples, the background expected in the signal region of data is estimated from the sideband regions in the M_{BC} and δM distributions of data. The distribution of M_{BC} in the sideband regions of data are extrapolated into the signal region (using an assumed fit shape common across modes that incorporates the natural threshold of the M_{BC}) to estimate the background b_{ee}^i . The shape is illustrated in Fig. 1(a). A similar extrapolation is done in the δM distribution and the difference between this and the M_{BC} estimate is taken as the systematic uncertainty inherent in our procedure. The estimated background for each mode is presented in Table I as b_{ee}^i where the statistical uncertainty is determined from the fit shape and number of events in the sideband regions.

The Poisson probability for the estimated background, which is modeled as a normal distribution that includes statistical and systematic uncertainties, to fluctuate up to the observed yield or higher gives us the signal significance. The combined signal significance for all modes is estimated to be 5.3σ . The individually most significant

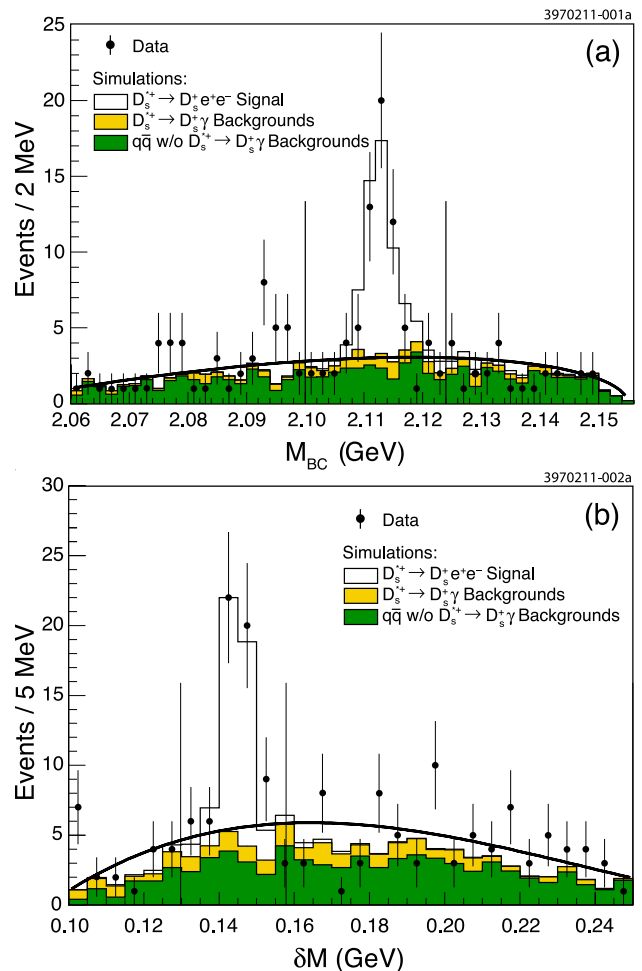


FIG. 1. Distributions of (a) M_{BC} and (b) δM in data and simulated samples summed over all nine D_s^+ decay modes used in this analysis. In each figure, the points with error bars are data, and the unshaded histogram is the simulated $D_s^{*+} \rightarrow D_s^+ e^+ e^-$ signal. Background events in the upper shaded histogram (yellow online) are from simulated $D_s^{*+} \rightarrow D_s^+ \gamma$ decays. Background events in the lower shaded histogram (green online) are from simulated $q\bar{q}$ events that do not include $D_s^{*+} \rightarrow D_s^+ \gamma$ or $D_s^{*+} \rightarrow D_s^+ e^+ e^-$. The curves are the fits of data to background shapes described in the text. The regions 2.100 to 2.124 GeV in (a), and 0.1298 to 0.1578 GeV in (b) are avoided in the shape fits to prevent contamination of the background estimates with signal events.

mode is $K^+ K^- \pi^+$ at 5.0σ .

The criteria for selecting $D_s^{*+} \rightarrow D_s^+ \gamma$ events are almost identical to those for $D_s^{*+} \rightarrow D_s^+ e^+ e^-$. First, the requirement for the presence of an $e^+ e^-$ pair is replaced with one for the presence of a photon candidate which must have an electromagnetic shower in the calorimeter of lateral spread narrower than that of 99% of true photons. Second, the δM criterion is broadened to compensate for the degradation in mass resolution caused by the replacement of the $e^+ e^-$ pair by a photon. Third, the criterion on M_{BC} range is dropped; its distribution

TABLE I. The yields y_{ee}^i , estimated backgrounds b_{ee}^i , background-subtracted yields n_{γ}^i , ratios of detection efficiencies ξ^i , and values R_{ee}^i of R_{ee} for each D_s^+ decay mode i . The uncertainties given for ξ^i are statistical only. The values of y_{ee}^i and b_{ee}^i are summed over all modes, while the ratio of branching fractions R_{ee} is computed using Eq. (3).

i	y_{ee}^i	b_{ee}^i	n_{γ}^i	ξ^i	R_{ee}^i (%)
$K^+K^-\pi^+$	14	$1.05^{+0.42}_{-0.33} \pm 0.79$	$9114 \pm 110 \pm 201$	4.65 ± 0.12	$0.66^{+0.21}_{-0.18}$
$K^+K^-\pi^+\pi^0$	6	$1.70^{+0.52}_{-0.43} \pm 0.56$	$3592 \pm 118 \pm 72$	4.80 ± 0.21	$0.58^{+0.38}_{-0.29}$
$K_S^0K^+$	1	$0.85^{+0.50}_{-0.36} \pm 0.74$	$1902 \pm 57 \pm 45$	4.31 ± 0.13	$0.03^{+0.33}_{-0.18}$
$K_S^0K^-\pi^+\pi^+$	4	$1.58^{+0.59}_{-0.47} \pm 0.40$	$1570 \pm 74 \pm 13$	5.38 ± 0.20	$0.83^{+0.83}_{-0.60}$
$\pi^+\pi^-\pi^+$	7	$1.57^{+0.50}_{-0.41} \pm 0.59$	$2745 \pm 93 \pm 52$	4.62 ± 0.10	$0.91^{+0.51}_{-0.40}$
$\eta\pi^+$	4	$1.40^{+0.82}_{-0.59} \pm 0.49$	$1037 \pm 46 \pm 37$	3.87 ± 0.10	$0.97^{+0.93}_{-0.67}$
$\eta\rho^+$	7	$2.62^{+0.63}_{-0.54} \pm 0.23$	$3170 \pm 161 \pm 313$	5.82 ± 0.24	$0.80^{+0.56}_{-0.44}$
$\eta'\pi^+; \eta' \rightarrow \pi^+\pi^-\eta$	4	$0.00^{+0.72}_{-0.00} \pm 0.00$	$691 \pm 34 \pm 40$	3.96 ± 0.12	$2.30^{+1.50}_{-0.97}$
$\eta'\pi^+; \eta' \rightarrow \rho^0\gamma$	4	$1.84^{+0.54}_{-0.45} \pm 0.25$	$1531 \pm 80 \pm 122$	4.97 ± 0.14	$0.70^{+0.78}_{-0.57}$
All Modes	51	$12.61^{+1.78}_{-1.29} \pm 4.05$			$0.72^{+0.15}_{-0.13}$

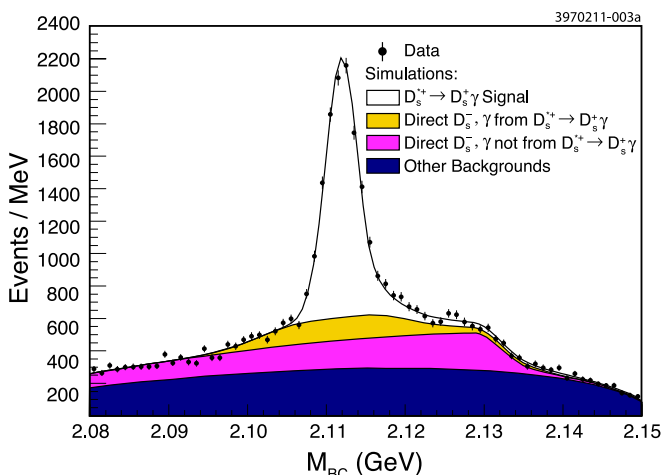


FIG. 2. Distribution of M_{BC} of $D_s^{*+} \rightarrow D_s^+\gamma$ events where $D_s^+ \rightarrow K^+K^-\pi^+$. The points with error bars are data, the unshaded region is the $D_s^{*+} \rightarrow D_s^+\gamma$ signal. Background events in the highest shaded region (magenta online) are events with a direct D_s^- paired with a photon from the $D_s^{*+} \rightarrow D_s^+\gamma$ decay. Background events in the middle shaded region (yellow online) are events with a direct D_s^- paired with a photon that did not come from $D_s^{*+} \rightarrow D_s^+\gamma$. Background events in the lowest shaded region (cyan online) are from all other sources.

is instead fit for signal yield using background and signal shapes determined from simulated samples as shown in Fig. 2 for the $K^+K^-\pi^+$ mode. These selection criteria are applied to simulated samples of $D_s^{*+} \rightarrow D_s^+\gamma$ to obtain their efficiencies for accepting signal events ϵ_{γ}^i , and on data to obtain the signal yields n_{γ}^i as listed in Table I.

The distribution of the e^+e^- invariant mass M_{ee} for the 51 observed events in the signal region is compared with that expected in our simulations and presented in Fig. 3. The distributions are found to be in good agree-

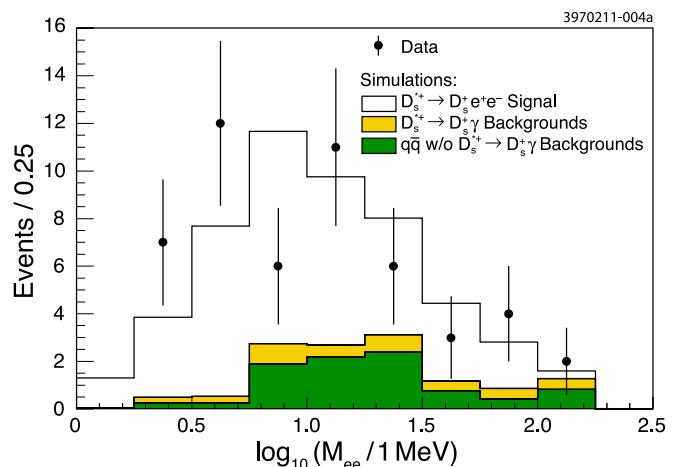


FIG. 3. Distribution of M_{ee} in simulated events within the signal region overlaid with the 51 events observed in data. The interpretations of the various simulation histograms are identical to those in Fig. 1.

ment with a Kolmogorov probability of 0.86 for the events to have come from the same distribution.

For each of the D_s^+ decay modes i , we calculate $R_{ee}^i = (y_{ee}^i - b_{ee}^i)/(n_{\gamma}^i/\xi^i)$, in which $\xi^i \equiv \epsilon_{\gamma}^i/\epsilon_{ee}^i$ is the ratio of radiative-to-Dalitz D_s^{*+} decay mode selection efficiencies as determined from MC samples. The resulting values of ξ^i and R_{ee}^i are shown in Table I. Note that the values of ξ^i are all equal to within $\pm 20\%$ because the dominant difference in efficiency is due to the photon versus e^+e^- selection criteria that are identical for all modes. The ξ^i vary somewhat with i due to the broadened δM windows and signal shape M_{BC} fit (instead of a fixed window) for the radiative D_s^{*+} modes relative to those of the Dalitz decays. Hence most systematic uncertainties in ξ^i due to D_s^+ selection cancel; *e.g.* those due to track-finding, particle identification, and selection of photons, π^0 s, K_S^0

decays, *etc.* We calculate R_{ee} for the sum of all modes by weighting the individual R_{ee}^i by the expected number of Dalitz decays in order to minimize the overall statistical uncertainty, obtaining

$$R_{ee} = \frac{\sum_i (n_\gamma^i / \xi^i) R_{ee}^i}{\sum_i n_\gamma^i / \xi^i} = \frac{\sum_i y_{ee}^i - b_{ee}^i}{\sum_i n_\gamma^i / \xi^i}, \quad (3)$$

which preserves the systematic error cancellation inherent in the use of ξ^i .

We consider systematic uncertainties of the signal yields and efficiencies in our measurement of R_{ee} . The systematic uncertainty in b_{ee}^i contributes a fractional uncertainty of 10.6%. Systematic uncertainties in n_γ^i and statistical uncertainties in ξ^i contribute a total fractional systematic uncertainty of 2.0%. Most systematic uncertainties in the ratio ξ^i cancel because the D_s^+ part of the selection is essentially identical for the $D_s^{*+} \rightarrow D_s^+ e^+ e^-$ and the $D_s^{*+} \rightarrow D_s^+ \gamma$. Two uncertainties remain. First, an uncertainty due to the different selection criteria on M_{BC} and δM , as described above, which is estimated to be 4.1%. Second, the uncertainty in the ratio of reconstructing an $e^+ e^-$ pair to that of a γ . The uncertainty in this ratio is estimated by studying the decay of $\psi(2S)$ mesons to $J/\psi \pi^0 \pi^0$. The ratio between the number of events where one of the π^0 decays to $\gamma e^+ e^-$ and the number of events where both π^0 decay to $\gamma \gamma$ must be equal to twice the ratio of branching fractions $R_{ee}^{\pi^0} \equiv \mathcal{B}(\pi^0 \rightarrow \gamma e^+ e^-) / \mathcal{B}(\pi^0 \rightarrow \gamma \gamma)$. Using this relationship, we measure $R_{ee}^{\pi^0} = (1.235 \pm 0.051)\%$ in a manner similar to R_{ee} by reconstructing the $J/\psi \pi^0 \pi^0$ through these two decay modes of the π^0 . We restrict the energies of the e^\pm to the range 10 to 144 MeV (the mass difference $m_{D_s^*} - m_{D_s}$). Compared to the known value of $(1.188 \pm 0.035)\%$ [2], we estimate the fractional systematic uncertainty on the ratio of efficiencies to be 6.5%. These fractional systematic uncertainties are combined in quadrature to give us the final result for the ratio R_{ee} in Eq. (4).

$$R_{ee} = [0.72_{-0.13}^{+0.15}(\text{stat}) \pm 0.10(\text{syst})]\% \quad (4)$$

This result leads to a re-evaluation of the known branching fractions of the D_s^{*+} meson as presented in Table II.

In summary, we report the first observation of a third decay mode of the D_s^{*+} , the $D_s^{*+} \rightarrow D_s^+ e^+ e^-$. We ob-

serve 51 candidate events in our signal region with an expected background of 12.6 events. The signal significance is estimated to be 5.3σ . The ratio of branching fractions $\mathcal{B}(D_s^{*+} \rightarrow D_s^+ e^+ e^-) / \mathcal{B}(D_s^{*+} \rightarrow D_s^+ \gamma)$ is measured as presented in Eq. (4) and found to be consistent with our theoretical prediction.

We gratefully acknowledge the effort of the CESR staff in providing us with excellent luminosity and running conditions. This work was supported by the A.P. Sloan Foundation, the National Science Foundation, the U.S.

TABLE II. Branching fractions in percent for the known decays of the D_s^{*+} meson from PDG 2010 [2], which assumed $\mathcal{B}(D_s^{*+} \rightarrow D_s^+ e^+ e^-) = 0$, and our re-evaluation using the value of R_{ee} reported in this Letter.

Decay Mode	PDG 2010	This Analysis
$D_s^{*+} \rightarrow D_s^+ \gamma$	94.2 ± 0.7	$93.5 \pm 0.5 \pm 0.5$
$D_s^{*+} \rightarrow D_s^+ \pi^0$	5.8 ± 0.7	$5.8 \pm 0.4 \pm 0.5$
$D_s^{*+} \rightarrow D_s^+ e^+ e^-$	0	$0.67_{-0.12}^{+0.14} \pm 0.09$

Department of Energy, the Natural Sciences and Engineering Research Council of Canada, and the U.K. Science and Technology Facilities Council.

-
- [1] R. H. Dalitz, Proc. Phys. Soc. A **64**, 667 (1951).
 - [2] K. Nakamura *et al.* (Particle Data Group), J. Phys. G **37**, 075021 (2010).
 - [3] S. Das, *Observation of the Dalitz decay of the first excited state of the charmed-strange meson*, Ph.D. thesis, Cornell University (2011).
 - [4] J. Gronberg *et al.* (CLEO Collaboration), Phys. Rev. Lett. **75**, 3232 (1995), arXiv:hep-ex/9508001.
 - [5] L. Landsberg, Phys. Rept. **128**, 301 (1985).
 - [6] Y. Kubota *et al.* (CLEO Collaboration), Nucl. Instrum. Meth. A **320**, 66 (1992).
 - [7] D. Peterson *et al.*, Nucl. Instrum. Meth. A **478**, 142 (2002).
 - [8] S. Dobbs *et al.* (CLEO Collaboration), Phys. Rev. D **76**, 112001 (2007), arXiv:0709.3783 [hep-ex].
 - [9] M. Artuso *et al.*, Nucl. Instrum. Meth. A **554**, 147 (2005), arXiv:physics/0506132.
 - [10] J. P. Alexander *et al.* (CLEO Collaboration), Phys. Rev. Lett. **100**, 161804 (2008), arXiv:0801.0680 [hep-ex].